Title

Distinct spatiotemporal patterns of neuronal functional connectivity in primary progressive aphasia variants

Journal

Brain, 140(10)

ISSN

0006-8950

Authors

Ranasinghe, Kamalini G
Hinkley, Leighton B
Beagle, Alexander J
et al.

Publication Date

2017-10-01

DOI

10.1093/brain/awx217

Peer reviewed

doi:10.1093/brain/awx217 BRAIN 2017: 140; 2737–2751 | 2737

BRAIN
A JOURNAL OF NEUROLOGY

Distinct spatiotemporal patterns of neuronal functional connectivity in primary progressive aphasia variants

Kamalini G. Ranasinghe,[1] Leighton B. Hinkley,[2] Alexander J. Beagle,[1] Danielle Mizuiri,[2] Susanne M. Honma,[2] Ariane E. Welch,[1] Isabel Hubbard,[1] Maria Luisa Mandelli,[1] Zachary A. Miller,[1] Coleman Garrett,[2] Alice La,[1] Adam L. Boxer,[1] John F. Houde,[2,3] Bruce L. Miller,[1] Keith A. Vossel,[1] Maria Luisa Gorno-Tempini[1,*] and Srikantan S. Nagarajan[2,3,*]

*These authors contributed equally to this work.

Primary progressive aphasia is a syndrome characterized by progressive loss of language abilities with three main phenotypic clinical presentations, including logopenic, non-fluent/agrammatic, and semantic variants. Previous imaging studies have shown unique anatomic impacts within language networks in each variant. However, direct measures of spontaneous neuronal activity and functional integrity of these impacted neural networks in primary progressive aphasia are lacking. The aim of this study was to characterize the spatial and temporal patterns of resting state neuronal synchronizations in primary progressive aphasia syndromes. We hypothesized that resting state brain oscillations will show unique deficits within language network in each variant of primary progressive aphasia. We examined 39 patients with primary progressive aphasia including logopenic variant ($n = 14$, age = 61 ± 9 years), non-fluent/agrammatic variant ($n = 12$, age = 71 ± 8 years) and semantic variant ($n = 13$, age = 65 ± 7 years) using magnetoencephalographic imaging, compared to a control group that was matched in age and gender to each primary progressive aphasia subgroup ($n = 20$, age = 65 ± 5 years). Each patient underwent a complete clinical evaluation including a comprehensive battery of language tests. We examined the whole-brain resting state functional connectivity as measured by imaginary coherence in each patient group compared to the control cohort, in three frequency oscillation bands—delta-theta (2–8 Hz); alpha (8–12 Hz); beta (12–30 Hz). Each variant showed a distinct spatiotemporal pattern of altered functional connectivity compared to age-matched controls. Specifically, we found significant hyposynchrony of alpha and beta frequency within the left posterior temporal and occipital cortices in patients with the logopenic variant, within the left inferior frontal cortex in patients with the non-fluent/agrammatic variant, and within the left temporo-parietal junction in patients with the semantic variant. Patients with logopenic variant primary progressive aphasia also showed significant hypersynchrony of delta-theta frequency within bilateral medial frontal and posterior parietal cortices. Furthermore, region of interest-based analyses comparing the spatiotemporal patterns of variant-specific regions of interest identified in comparison to age-matched controls showed significant differences between primary progressive aphasia variants themselves. We also found distinct patterns of regional spectral power changes in each primary progressive aphasia variant, compared to age-matched controls. Our results demonstrate neurophysiological signatures of network-specific neuronal dysfunction in primary progressive aphasia variants. The unique spatiotemporal patterns of neuronal synchrony signify diverse neurophysiological disruptions and pathological underpinnings of the language network in each variant.

1 Memory and Aging Center, Department of Neurology, University of California San Francisco, San Francisco, CA 94158, USA
2 Biomagnetic Imaging Laboratory, Department of Radiology and Biomedical Imaging, University of California San Francisco, San Francisco CA 94143, USA

Received February 18, 2017. Revised June 28, 2017. Accepted July 4, 2017. Advance Access publication August 31, 2017

3 Speech Neuroscience Laboratory, Department of Otolaryngology, Head and Neck Surgery, University of California San Francisco, San Francisco CA 94143, USA

Correspondence to: Srikantan S. Nagarajan, PhD
Biomagnetic Imaging Laboratory, Department of Radiology and Biomedical Imaging, University of California, San Francisco, 513 Parnassus Avenue, S362, San Francisco, CA 94143-0628, USA
E-mail: sri@ucsf.edu

Keywords: magnetoencephalography; primary progressive aphasia; resting state functional connectivity; neural oscillations; dementia

Abbreviations: lvPPA = logopenic variant PPA; MEGI = magnetoencephalographic imaging; nfvPPA = non-fluent/agrammatic variant PPA; PPA = primary progressive aphasia; svPPA = semantic variant PPA

Introduction

Primary progressive aphasia (PPA) is a clinical syndrome where speech and language impairments are the predominant neurobehavioural deficits (Mesulam, 2003; Mesulam *et al.*, 2014). Three main clinical phenotypes of PPA have been identified, each with a distinct deficit in language function: logopenic variant (lvPPA), characterized by prominent phonological impairments; semantic variant (svPPA), characterized by loss of word comprehension and object concepts; and non-fluent/agrammatic variant (nfvPPA), characterized by impaired motor speech and/or grammatical processing (Gorno-Tempini *et al.*, 2011). Each PPA variant shows a unique anatomical pattern of neuronal loss—left posterior temporo-parietal atrophy in lvPPA, anterior temporal lobe atrophy in svPPA, and left posterior fronto-insular and subcortical atrophy in nfvPPA (Galantucci *et al.*, 2011; Grossman, 2012; Mandelli *et al.*, 2014; Leyton *et al.*, 2016). Collectively the anatomical patterns of atrophy in PPA encompass the language network of the brain. Functional neuroimaging studies have demonstrated abnormal blood oxygen level-dependent signal changes, disrupted white matter tracts, and altered metabolic profiles within the language network in PPA patients (Sonty *et al.*, 2007; Wilson *et al.*, 2010; Guo *et al.*, 2013; Lehmann *et al.*, 2013). Further, post-mortem neuropathological and *in vivo* neuroimaging studies have identified Alzheimer's disease-related molecular changes in lvPPA and frontotemporal degeneration-type protein depositions in nfvPPA and svPPA, suggesting selective vulnerability of each involved language circuit (Rabinovici *et al.*, 2008; Grossman, 2010; Ossenkoppele *et al.*, 2016). Despite these important advances in the field of PPA, the electrophysiological properties of altered temporal dynamics of neurons within affected brain circuits remain largely unknown. The neural signatures of disrupted coordinated activity within the language network are prime candidates for understanding the mechanisms linking molecular pathology and system-level functional deficits in PPA.

Magnetoencephalographic imaging (MEGI) allows non-invasive mapping of neural oscillations in the brain with high temporal and spatial resolution. Coupled with source space reconstruction algorithms, MEGI is ideally suited to characterize neuronal oscillations with millisecond precision. Oscillations are a fundamental property of cortical networks and represent the coordinated activity of neurons either within local ensembles or as long-range connections. These rhythmic patterns are typically segregated into distinct frequency bands as delta (1–4 Hz), theta (4–8 Hz), alpha (8–12 Hz), beta (12–30 Hz), and gamma (>40 Hz). Electrophysiological properties of different low and high frequency oscillations have shown to be associated with specific cellular and synaptic processes including pacemaker currents and reciprocal coupling of excitatory and inhibitory neurons (Buzsaki, 2011; Buzsaki *et al.*, 2012). Neurophysiological recordings in humans as well as in non-human primates have demonstrated that spatiotemporal patterns of correlated oscillations relate to canonical computations of underlying cognitive processes (Harris and Gordon, 2015). In particular, spontaneous oscillations of the resting brain have been reliably mapped onto large-scale functional neural networks (de Pasquale *et al.*, 2012). Altered spectral patterns and impaired coherence of oscillations have been identified as indicators of network dysfunctions underlying specific cognitive deficits in Alzheimer's disease, frontotemporal dementia, schizophrenia, and autism spectrum disorders (Hinkley *et al.*, 2010; Hughes and Rowe, 2013; Khan *et al.*, 2013; Ranasinghe *et al.*, 2014).

In this study, we investigated the resting brain oscillations in PPA patients compared to an age-matched control population using MEGI. We examined the functional connectivity patterns based on neuronal synchrony within delta-theta, alpha and beta frequency bands, using an unbiased whole-brain approach. We also examined the spectral power changes within each frequency. We hypothesized that PPA patients will show significant oscillatory changes and that each PPA variant will be characterized by distinct spatiotemporal patterns of altered neuronal synchrony.

Materials and methods

Subjects

Participants were recruited from research cohorts at the University of California San Francisco (UCSF) Memory and

Aging Center and consisted of 39 patients meeting the diagnostic criteria for PPA ($n = 14$ lvPPA; $n = 13$ svPPA; $n = 12$ nfvPPA) (Mesulam, 2001) and 20 age-matched controls. Each PPA patient was assigned to their specific variant according to the current diagnostic criteria (Gorno-Tempini *et al.*, 2008, 2011). All patients underwent a complete clinical history, physical examination, and neuropsychological evaluation. All participants underwent a 4–10 min session of magnetoencephalogram (MEG) recording at rest and structural MRI of the brain. Eligibility criteria for age-matched controls included normal cognitive performance, normal MRI, and absence of neurological, psychiatric, or other major medical illnesses. Informed consent was obtained from all participants or their assigned surrogate decision-makers. The study was approved by the UCSF institutional review board for human research.

Neuropsychological assessment

For each patient, a structured caregiver interview documented the Clinical Dementia Rating scale (CDR). Each patient was assessed by a Mini-Mental State Examination (MMSE) and a battery of neuropsychological tests (Kramer *et al.*, 2003; Ranasinghe *et al.*, 2016) (Supplementary material).

Comparison of demographic and cognitive variables

Statistical tests comparing demographic and cognitive abilities were performed using SAS (SAS 9.4; SAS Institute, Cary, NC). Age was compared using one-way ANOVA with Dunnett's *post hoc* comparison. Wilcoxon-Mann-Whitney test was used to compare education between each patient group and the control group. Fisher exact test was used to compare sex, handedness, and race between each patient group and the control group. Neuropsychological test scores were compared across the PPA variants using one-way ANOVA and Tukey *post hoc* comparison.

MRI acquisition and voxel-based morphometry analysis

Structural brain images were acquired using a unified MRI protocol on a 3 T Siemens MRI scanner at the Neuroscience Imaging Center (NIC) at UCSF, within 47 ± 78 days of the MEG evaluation. Structural MRIs were used to generate the head model for source space reconstruction of MEG sensor data, and to generate grey matter volume estimates (Supplementary material). Voxel-based morphometry-derived volumes were used for statistical corrections of functional connectivity and spectral power estimates derived from MEGI (described below).

Resting state MEG data acquisition

Each subject underwent MEG recording on a 275-channel whole-head biomagnetometer system consisting of 275 axial gradiometers (MISL, Coquitlam, British Columbia, Canada). Three fiducial coils including nasion and left and right pre-auricular points were placed to localize the position of head relative to sensor array, and later co-registered to each individual's respective MRI to generate an individualized head shape. Data collection was optimized to minimize within-session head movements and to keep it below 0.5 cm. Continuous recording (4–10 min) was collected from each subject while lying supine and awake with eyes closed (sampling rate: 600 Hz). We selected a 1-min continuous segment with minimal artefacts (i.e. minimal excessive scatter at signal amplitude < 10 pT), for each subject, for analysis. The study protocol required the participant to be interactive with the investigator and be awake at the beginning of the data collection. Spectral analysis of each recording was visually inspected and those showing known electrophysiological features of sleep were excluded. Artefact detection was confirmed by visual inspection of sensor data and channels with excessive noise within individual subjects were removed prior to analysis. Both controls' and patients' data were within our specified limits of signal scatter, and were not different in the degree of head movement [unpaired *t*-test: $t = 1.5$, $P = 0.13$; mean $\pm$ standard deviation (SD), for patients = 0.32 ± 0.23 cm; controls = 0.22 ± 0.23 cm].

Source space reconstruction of MEG data

Tomographic reconstructions of the MEG data were generated using a head model based on each participant's structural MRI. Spatiotemporal estimates of neural sources were generated using a time–frequency optimized adaptive spatial filtering technique implemented in the Neurodynamic Utility Toolbox for MEG (NUTMEG; http://nutmeg.berkeley.edu). Tomographic volume of source locations (voxels) was computed through an adaptive spatial filter (10 mm lead field) that weights each location relative to the signal of the MEG sensors (Dalal *et al.*, 2008, 2011). The source space reconstruction approach provided amplitude estimations at each voxel derived through the linear combination of spatial weighing matrix with the sensor data matrix (Dalal *et al.*, 2008). We used lead-field (column) normalization to account for the reconstruction power bias towards the centre of the head. A high resolution anatomical MRI for each subject was spatially normalized to the Montreal Neurological Institute (MNI) template using statistical parametric mapping version 8 software (SPM8, http://www.fil.ion.ucl.ac.uk/spm/software/spm8/), and the resulting transformation parameters were applied to each individual subjects' source reconstruction maps.

Functional connectivity and spectral power estimation

We computed imaginary coherence for each subject, at each frequency band (2–8 Hz, delta-theta; 8–12 Hz, alpha; 12–30 Hz, beta) between all pairs of voxels. Imaginary coherence captures only the coherence that cannot be explained by volume spread (Nolte *et al.*, 2004), and is a reliable metric for resting state functional connectivity analyses (Guggisberg *et al.*, 2008; Martino *et al.*, 2011; Hinkley *et al.*, 2012; Engel *et al.*, 2013). We computed the global connectivity at each voxel as the average of the Fisher's Z-transformed absolute value of the imaginary coherence between a given voxel (10 mm isotropic) and all other voxels in the grid.

We also examined the spectral power maps using the source space reconstructed data. Each subjects' reconstruction, within each frequency, was spatially normalized to standard MNI template by applying the transformation matrix from the

structural MRI. Source spectral power density for each location was derived through a noise-corrected power density statistic for the signal magnitude in each frequency band during the 60-s experimental time window.

Whole-brain analyses between each PPA variant and controls

Using statistical non-parametric whole-brain mapping methods incorporated in the NUTMEG toolbox (Dalal *et al.*, 2008, 2011), we examined the differences between each PPA variant and age-matched controls in: (i) functional connectivity (i.e. imaginary coherence); and (ii) spectral power. To minimize spatial frequency noise in the beamformer volumes, average and variance maps for each individual frequency band were smoothed using a Gaussian kernel with a width of $20 \times 20 \times 20$ mm full-width at half-maximum (Barnes *et al.*, 2004). Statistical significance was estimated by obtaining a permuted distribution (through 2^N possible combinations of negations) and estimating the significance of the test statistic (imaginary coherence or spectral power) value from its position in this permuted distribution. Multiple comparisons were corrected using cluster correction procedures in NUTMEG (Dalal *et al.*, 2011; Kort *et al.*, 2016) with a cut-off level of 20 voxels (only the clusters with 20 congruent voxels remained), and *P*-values thresholded to $P < 0.05$. When effects were significant, we applied more stringent thresholds of $P < 0.01$ or 0.001 in order to yield the most robust effects. We report the most conservative threshold producing significant effects. The specific thresholds used in each comparison are noted in the figure legends. In the cluster correction, following permutation testing, a voxel cluster was considered significant if there were more contiguous voxels within a cluster after passing a statistical (*P*-value) threshold. Clusters in the thresholded statistical maps were discarded if they fell below the 95% of null-distribution cut-off following permutation testing and did not meet the required minimum value of contiguous 20 voxels. This approach sufficiently minimized the possibility of observing spurious effects. The images were thresholded such that only the voxels that exceeded the significance threshold can be seen in the figures.

Region of interest-based analyses

Suprathreshold clusters from the comparisons between each PPA variant and controls, at each frequency, served as non-contiguous variant-specific regions of interest for the subsequent analyses. In these region of interest-based analyses, we first examined the functional connectivity and spectral power after accounting for the grey matter volume loss in the corresponding variant-specific regions of interest. Next, we compared the functional connectivity patterns within variant-specific regions of interest directly between PPA variants.

Regional grey matter volume correction for functional connectivity and spectral power deficits

To examine whether the MEGI-derived functional connectivity deficits within the variant-specific regions of interest in each PPA variant were significant after correcting for atrophy, we used a general linear model and included cortical grey matter volume of the corresponding variant-specific region of interest as a covariate. A separate model was used for each PPA variant versus control comparison, at each frequency. The step-by-step details are as follows: first, we extracted the mean imaginary coherence for each variant-specific region of interest (at a given frequency band), for each subject. Next, we extracted the mean voxel-based morphometry-derived grey matter volume of the corresponding variant-specific region of interest, for each subject. Using PROC GLM in SAS, we then ran a general linear model and included the voxel-based morphometry-derived volume as a covariate. The model equation was as follows: *MEGI-derived imaginary coherence = Group + VBM-derived volume + E*, where 'Group' indicates the categorical label indicating PPA variant or control, and *E* indicates the model error. Inclusion of additional covariates of age and gender into the model did not affect our results, and therefore we report results here without these additional covariates. Identical methodology was used, including spectral power as the dependent variable to examine the effects after controlling for grey matter volume.

Statistical comparison of functional connectivity patterns between PPA variants

We used two separate approaches to examine whether the MEGI-derived functional connectivity pattern observed when each PPA variant was compared to age-matched controls are significantly different between the PPA variants themselves. In the first analysis, we used a general linear model where MEGI-derived functional connectivity was the dependent variable and PPA variant identity was the predictor variable. In the second analysis, we used a logistic regression model where PPA variant identity was the dependent variable and MEGI-derived functional connectivity was the predictor variable. For both approaches, we first extracted the mean imaginary coherence for each of the nine variant-specific regions of interest (for each PPA syndrome at each frequency), for each patient. A separate model was used at each frequency band, in each approach.

The general linear model (PROC GLM in SAS) tested whether each pair of PPA variants were different from each other based on imaginary coherence within the variant-specific regions of interest of the given pair. Specifically, we used a two-way ANOVA model, including PPA variant identity and variant-specific region of interest identity as predictor variables, and the MEGI-derived imaginary coherence of the variant-specific region of interest is the dependent variable. The model equation was as follows: *MEGI-derived imaginary coherence = Group + variant-specific-region of interest + E*, where 'Group' indicates categorical label of the PPA variant; 'variant-specific region of interest' indicates categorical label of the variant-specific region of interest, and *E* indicates model error.

The logistic regression-based discriminant analysis (PROC LOGISTIC in SAS) quantified the extent of distinction between each pair of PPA variants based on imaginary coherence within the variant-specific regions of interest of the given pair. The imaginary coherence values of the PPA pair comprised the predictor variables of the model, and the category identity of the PPA variant was the dependent variable. Receiver operating characteristic (ROC) plots were constructed to quantify the confidence limits of each pairwise comparison.

Results

Demographic characteristics and global cognitive assessment

Each PPA variant—lvPPA, svPPA, and nfvPPA—was demographically matched with the control group in their distribution of age, sex, handedness, race and education (Table 1). In pairwise comparisons, lvPPA patients were significantly younger than nfvPPA patients ($P < 0.05$). PPA variants showed comparable degrees of disease severity as measured by CDR (Table 2). The average MMSE of the combined cohort of patients was mild to moderately impaired (MMSE = 23.9 ± 4.8). In pairwise comparisons of MMSE scores, nfvPPA patients significantly outperformed both lvPPA and svPPA patients (Table 2).

Neuropsychological performance and grey matter atrophy in PPA variants

Each PPA variant showed unique deficits in language abilities. Patients with lvPPA showed predominant dysfunction in repetition, in both western aphasia and motor speech evaluation batteries (Table 2). Patients with nfvPPA showed predominant motor speech errors, and reported significantly higher dysarthria and speech apraxia ratings (Table 2). Patients with svPPA showed a predominant loss of semantic abilities with significantly poor confrontation naming and vocabulary performance (Table 2).

In standard bedside neuropsychological testing, the svPPA patients showed poor verbal memory abilities, but relatively better executive function, compared to lvPPA and nfvPPA patients (Table 2, pairwise comparisons of short delay and delayed California Verbal Learning Test, and set shifting). Patients with lvPPA as a group, showed the lowest scores in verbal working memory and phonological short term memory (Table 2).

Consistent with previous reports (Gorno-Tempini *et al.*, 2004), the grey matter volume compared to an age-matched control population, demonstrated characteristic patterns in each PPA variant (Supplementary Fig. 1). Patients with lvPPA showed a left predominant atrophy over the temporal and parietal lobes with the most significant volume loss over the posterior temporal cortex extending into the adjacent parietal cortex. Patients with svPPA showed a bilateral volume loss involving both anterior temporal lobes, albeit with a more extensive distribution in left temporal lobe. Patients with nfvPPA showed minimal cortical atrophy and mild-to-moderate subcortical volume loss, mainly involving the inferior frontal and pre-central regions in the left hemisphere, consistent with previous reports (Galantucci *et al.*, 2011; Leyton *et al.*, 2016).

Spatiotemporal patterns of functional connectivity disruptions in PPA variants

Neural synchronizations as measured by imaginary coherence, in control subjects, showed distinct spatiotemporal patterns (Supplementary Fig. 2). Delta-theta frequency (2–8 Hz) showed strong synchrony in parieto-occipital cortices extending into frontal cortices. Alpha (8–12 Hz) synchronizations were strongest in the occipital cortices, while beta (12–30 Hz) showed strongest synchronizations in the parietal cortices.

Confirming our initial hypothesis, each PPA variant demonstrated a distinct pattern of functional connectivity deficit compared to controls. As we present in detail below, alpha and beta oscillations consistently showed reduced functional connectivity (i.e. hyposynchrony) in all PPA variants, while delta-theta oscillations showed increased functional connectivity (i.e. hypersynchrony) in lvPPA and variable effects in nfvPPA and svPPA.

Unique patterns of left lateralized alpha and beta hyposynchrony in PPA variants

All three PPA variants showed alpha and beta hyposynchrony when compared to age-matched controls. In the

Table 1 Participant demographics

	lvPPA ($n = 14$)	nfvPPA ($n = 12$)	svPPA ($n = 13$)	Controls ($n = 20$)
Age (years)	60.9 ± 9.0	71.0 ± 7.7	65.4 ± 6.6	65.2 ± 5.4
Female sex, *n* (%)	9 (64.3)	7 (58.3)	7 (53.9)	13 (65.0)
Right handedness, *n* (%)	9 (64.3)	11 (91.7)	13 (100)	16 (80.0)
White race, *n* (%)[a]	11 (91.7)	10 (90.9)	11 (84.6)	18 (94.7)
Education, years	18 (14–20)	16 (15–18)	18 (16–20)	18 (16–19)
Disease duration, years	5.3 (2.2)	4.7 (1.9)	5.8 (2.5)	-

Values for age indicate means ± standard deviations of the participants at the time of evaluation. Values for education indicate medians with interquartile ranges within parentheses.
[a]Race was self-reported and the total number of observations reported for each group included, $n = 12$, $n = 11$, $n = 13$ and $n = 19$ for lvPPA, nfvPPA, svPPA, and control groups, respectively.
One-way ANOVA and Dunnett's *post hoc* comparison showed no significant difference of age between each patient group and the control group. Wilcoxon-Mann-Whitney test showed no significant difference of education between each patient group and the control group. Fisher exact test for sex, handedness, and race between each patient group and controls showed no statistical differences.

Table 2 Neuropsychological test performance

Variable	lvPPA (*n* = 14)	nfvPPA (*n* = 12)	svPPA (*n* = 13)
Global cognitive function			
MMSE	**21.4 ± 1.1**[a]	27.4 ± 1.2	**23.3 ± 1.2**[b]
CDR	0.6 ± 0.1	0.4 ± 0.1	0.7 ± 0.1
Language function			
WAB - Repetition	**72.0 ± 3.0**[c,d]	85.3 ± 3.3	91.8 ± 2.9
Repetition	**44.5 ± 2.2**[d]	**50.2 ± 2.8**[b]	59.8 ± 2.3
Speech Apraxia Rating	0.4 ± 0.5	**3.3 ± 0.5**[a,e]	0.2 ± 0.5
Dysarthria Rating	0.0 ± 0.5	**3.1 ± 0.5**[f,e]	0.2 ± 0.4
Syntax Comprehension	91.8 ± 4.8	83.9 ± 5.3	91.1 ± 4.6
Boston Naming Test	10.2 ± 0.9	11.7 ± 1.0	**4.9 ± 0.8**[d,e]
Peabody Picture Vocabulary Test	14.6 ± 0.9	13.5 ± 1.0	**8.0 ± 0.8**[d,e]
Category Fluency (animals/1 min)	8.3 ± 1.3	11.7 ± 1.5	8.2 ± 1.2
Visuospatial function			
Face discrimination (CATS – face matching)	11.5 ± 0.3	11.2 ± 0.3	11.5 ± 0.2
Visuoconstruction (Benson copy)	14.4 ± 0.5	14.4 ± 0.5	15.6 ± 0.4
Location discrimination (VOSP number location)	8.4 ± 0.6	8.6 ± 0.6	9.1 ± 0.5
Episodic memory function			
Visual free recall (Benson 10 min)	7.2 ± 1.1	9.7 ± 1.2	7.9 ± 1.0
Short delay verbal memory (CVLT 30 s)	4.1 ± 0.6	5.1 ± 0.7	**1.9 ± 0.6**[g,h]
Verbal free recall (CVLT 10 min)	3.6 ± 0.7	4.6 ± 0.8	**1.0 ± 0.6**[g,h]
Verbal recognition (CVLT recognition)	7.9 ± 0.5	7.9 ± 0.6	6.8 ± 0.5
Executive function and working memory			
Lexical fluency (D words/1 min)	7.4 ± 1.0	4.7 ± 1.2	7.9 ± 0.9
Design fluency	6.8 ± 0.9	5.6 ± 1.0	7.3 ± 0.8
Phonological short-term memory (Digits forward)	**3.8 ± 0.3**[d]	**4.5 ± 0.4**[b]	5.7 ± 0.3
Verbal working memory (Digits backward)	**2.9 ± 0.3**[g]	3.1 ± 0.4	4.0 ± 0.3
Set shifting (Modified trails – speed)	**0.2 ± 0.04**[i]	**0.2 ± 0.05**[b]	0.4 ± 0.04

CATS = Comprehensive Affect Testing System; CDR = Clinical Dementia Rating; CVLT = California Verbal Learning Test containing nine items; MMSE = Mini-Mental State Examination; VOSP = Visual Object and Space Perception; WAB = Western Aphasia Battery.

Values are least-square means ± standard deviation for each group adjusted for age and MMSE. Repetition, speech apraxia and dysarthria were evaluated using motor speech evaluation battery. Scores on the MMSE range from 0 to 30, with higher scores denoting better cognitive function. Scores on the CDR range from 0 to 3 with higher scores denoting greater impairment.

[a]$P < 0.01$ lvPPA versus nfvPPA.
[b]$P < 0.05$ svPPA versus nfvPPA.
[c]$P < 0.05$ lvPPA versus nfvPPA.
[d]$P < 0.001$ lvPPA versus svPPA.
[e]$P < 0.001$ svPPA versus nfvPPA.
[f]$P < 0.001$ lvPPA versus nfvPPA.
[g]$P < 0.05$ lvPPA versus svPPA.
[h]$P < 0.01$ svPPA versus nfvPPA.
[i]$P < 0.01$ lvPPA versus svPPA.

left hemisphere, the anatomical patterns of hyposynchrony corresponded to the language network and was uniquely affected in each PPA variant (Fig. 1A–C and Supplementary Table 1). In lvPPA patients, alpha hyposynchrony was found in the inferior temporal cortex, and beta hyposynchrony was found in the inferior temporal, posterior frontal, and lateral parietal cortices, in the left hemisphere. In contrast, nfvPPA patients showed alpha and beta hyposynchrony in the left inferior frontal gyrus, while svPPA patients showed alpha and beta hyposynchrony in the left posterior superior temporal and adjacent parietal cortices. As opposed to the left hemisphere, the anatomic distributions of functional connectivity deficits in the right hemisphere were less distinct between PPA variants. For example, lvPPA and svPPA did not show any alpha deficits in the right hemisphere, while all three groups showed an overlapping pattern of beta hyposynchrony involving the posterior parietal and temporal cortices (Fig. 1A–C), with the notable exception of spared right temporal lobe in svPPA (Fig. 1C). Collectively these results reveal unique patterns of left lateralized alpha and beta hyposynchrony involving the language network in each PPA variant.

Region of interest-based analyses of alpha and beta hyposynchrony

To ensure that functional connectivity deficits were not an epiphenomenon of cortical atrophy, we examined the imaginary coherence differences in each PPA variant against controls, using a general linear model in which grey matter volumes were included as a covariate. The alpha and beta

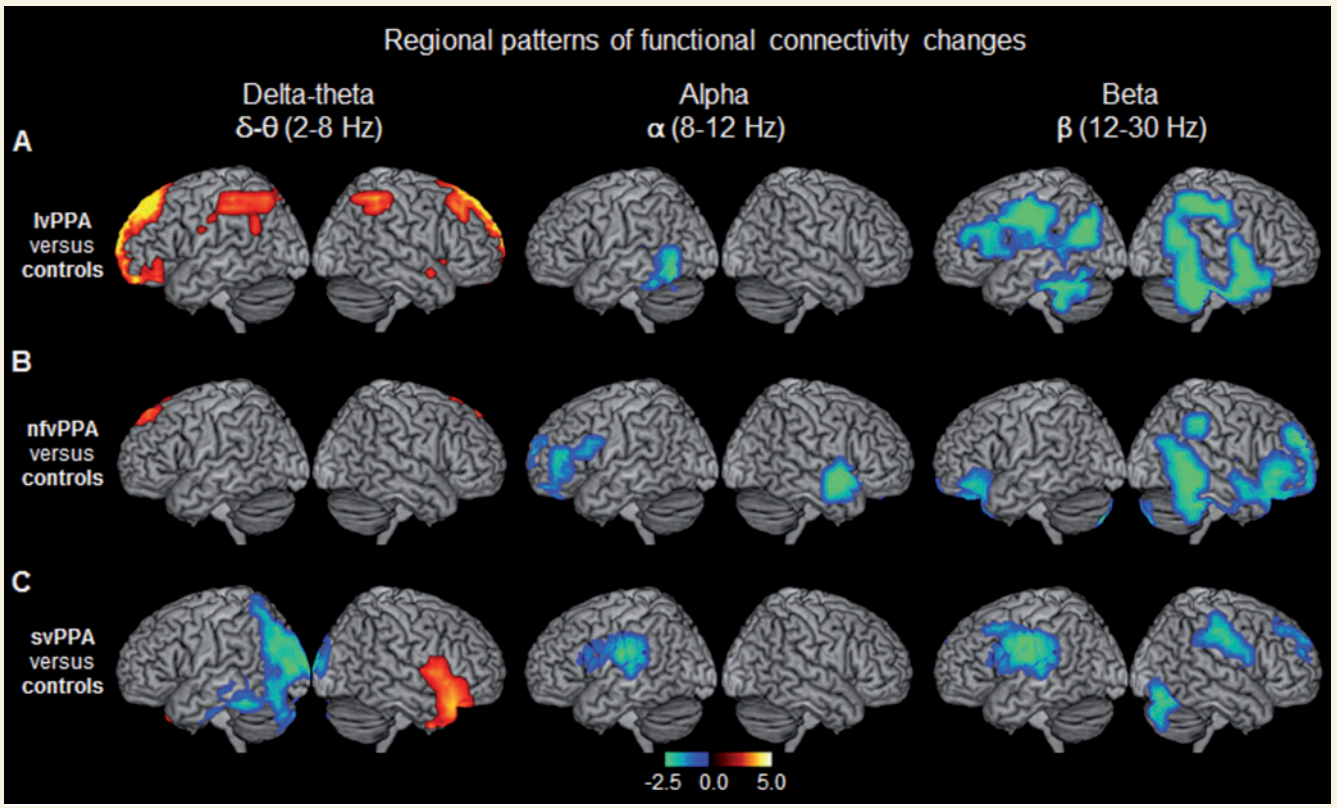

Figure 1 Spatiotemporal patterns of resting state functional connectivity in each PPA variant compared to age-matched controls. The rendering brain images depict the distinct patterns of global imaginary coherence differences within each frequency in the three PPA variants compared to age-matched controls. (**A**) lvPPA versus controls; (**B**) nfvPPA versus controls; (**C**) svPPA versus controls. Colours indicate *t*-values depicting statistically significant patterns of increased (hot colours) and decreased (cold colours) imaginary coherence compared to controls, within each frequency. From *left* to *right* each column represents frequency bands: delta-theta (2–8 HZ); alpha (8–12 Hz); beta (12–30 Hz), respectively. Images are statistically thresholded using cluster correction (20 voxels cut-off) and $P < 0.01$ for lvPPA, $P < 0.05$ for nfvPPA and svPPA ($n = 14$ lvPPA; $n = 13$ svPPA; $n = 12$ nfvPPA; $n = 20$ controls).

hyposynchrony in all three PPA variants remained statistically significant in this analysis (Fig. 2A–C), indicating that functional deficits that explicitly affect different network components are robust to structural volume loss.

Direct pairwise comparisons between PPA variants, using general linear models to predict alpha and beta imaginary coherence (with in variant-specific regions of interest) consistently showed significant group × variant-specific region of interest interactions (Table 3). A logistic regression-based discriminant analysis quantified the differences of alpha and beta imaginary coherence (within variant-specific regions of interest) between PPA variants, and demonstrated confidence intervals consistently > 0.5 for all pairwise comparisons (Fig. 3A–C). Taken together these results indicate that region-specific alpha and beta functional connectivity deficits are distinct between PPA variants.

Distinct patterns of delta-theta hypersynchrony in logopenic variant PPA

In contrast to alpha and beta hyposynchrony, lvPPA patients showed significantly increased functional connectivity (i.e. hypersynchrony) within delta-theta frequency over bilateral medial frontal cortices and posterior superior parietal cortices (Fig. 1A and Supplementary Table 1). Patients with nfvPPA also showed a very small cluster of voxels in the dorsal medial frontal cortex with delta-theta hypersynchrony compared to controls (Fig. 1B and Supplementary Table 1). Patients with svPPA, in contrast, showed both increased and decreased patterns of delta-theta synchrony—hypersynchrony in right anterior temporal and hyposynchrony in left posterior temporal/occipital cortices (Fig. 1C).

Region of interest-based analyses of delta-theta synchrony

After accounting for the cortical grey matter loss within the anatomic regions showing delta-theta hypersynchronous patterns found in lvPPA, the differences between the lvPPA and controls remained strongly significant (Fig. 2A). The delta-theta hypersynchrony found in nfvPPA also survived atrophy correction albeit at a lower statistical threshold (Fig. 2B). In contrast, the delta-theta synchrony changes in svPPA patients were no longer significant (Fig. 2C) after correcting for cortical atrophy. In

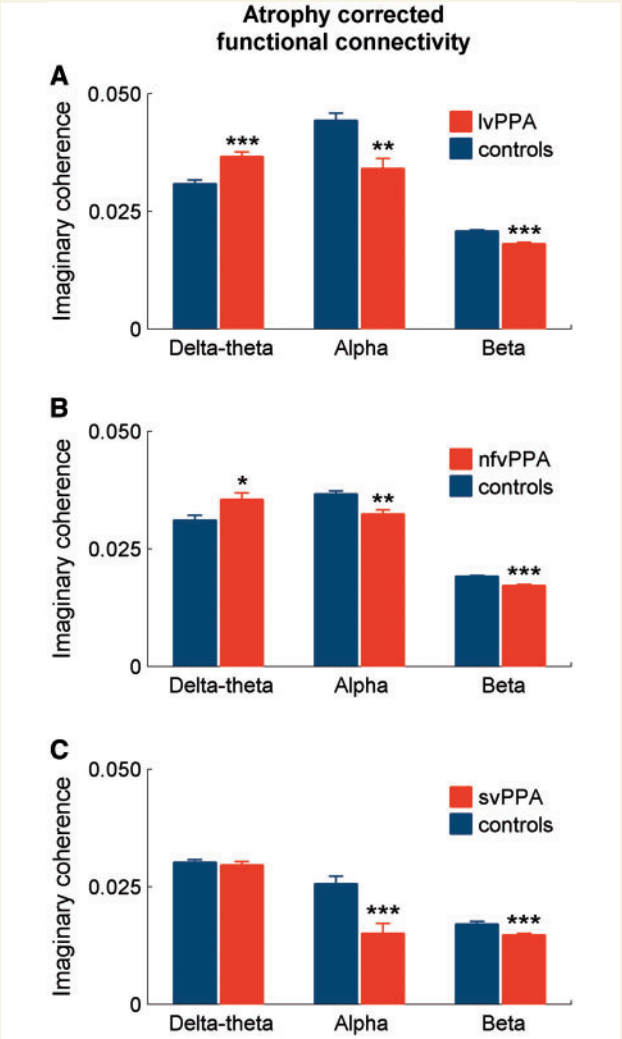

Figure 2 Patterns of functional connectivity differences after correcting for cortical atrophy. The bar plots depict the results from a general linear model analysis for imaginary coherence values including the cortical grey matter volumes as a covariate. The analysis was done for each frequency, comparing each PPA variant and controls. The stars indicate statistically significant differences between patients and controls. (**A**) lvPPA versus controls; (**B**) nfvPPA versus controls; (**C**) svPPA versus controls. *$P < 0.05$; **$P < 0.01$; ***$P < 0.001$.

summary, the delta–theta hypersynchrony showed a robust pattern in lvPPA and a weaker, limited pattern in nfvPPA.

The two-way ANOVA model based on delta-theta synchrony within variant-specific regions of interest also showed robust effects in pairwise comparisons between lvPPA against other two PPA variants. Specifically, the pairwise comparisons identified a significant Group effect in lvPPA versus nfvPPA and lvPPA versus svPPA comparisons (Table 3). However, in nfvPPA versus svPPA comparison, there were no significant group or interaction effects. Quantitative differences from logistic regression analysis of variant-specific region of interest-based delta-theta connectivity showed consistently larger (>0.5) confidence intervals at lvPPA versus other PPA variants and a marginally high confidence interval of 0.59 for nfvPPA versus svPPA comparison (Fig. 3). Collectively, these results indicate that lvPPA patients are distinctly different from the other two PPA variants based on the patterns of delta-theta hypersynchrony.

Spatiotemporal patterns of spectral power in PPA variants

Coherence analyses yield the degree of connectivity between neuronal ensembles and is mostly complementary to the patterns of power spectra representing the amplitudes of rhythmic activity (Bullmore and Sporns, 2009). However, a change in connectivity does not necessarily mean a change in activity. For example, within a given functional network, the former may represent the functional communication between nodes, while the latter may represent the focal activity within a node. Neuronal synchrony and spectral power hence provide two partially independent means capable of modulating the function of a cortical network. We next sought to examine the spectral power density within each frequency oscillation and their relative dependencies on cortical atrophy in each PPA variant.

In healthy elderly controls the spatial patterns of oscillatory power showed a posterior dominant distribution involving both hemispheres symmetrically (Supplementary Fig. 3). Both delta-theta and alpha frequencies showed the maximum spectral power density over the posterior parietal and occipital regions of the brain. Spectral power density of beta oscillations, on the other hand, showed maximum power over the parietal lobes. As we describe below, when compared to the patterns of healthy controls, PPA variants showed unique spatiotemporal patterns of altered spectral power.

Reduced alpha and beta spectral power in all three PPA variants

The spectral power changes within both alpha and beta bands were dominated by region-specific reductions in all three PPA subgroups. Patients with lvPPA showed significantly reduced power of alpha and beta in the posterior brain regions with a bilateral, left > right involvement (alpha: posterior temporal and occipital cortex; beta: posterior temporal, parietal and occipital cortex; Fig. 4A and Supplementary Table 3). Patients with nfvPPA also showed reduced alpha and beta power compared to controls. Reduced alpha power was limited to right hemisphere and involved the right inferior frontal gyrus and adjacent temporal cortex, while beta power was reduced bilaterally and involved both left and right inferior frontal gyri and adjacent temporal regions (Fig. 4B and Supplementary Table 3). The svPPA patients showed significantly reduced alpha power in both left and right anterior temporal lobes

Table 3 Two-way ANOVA of pairwise comparisons of functional connectivity patterns at each frequency

Pairwise comparison		Effect of Group (PPA variant) F-value (*P*-value)	Effect of variant-specific region of interest F-value (*P*-value)	Effect of interaction (variant-specific region of interest by Group) F-value (*P*-value)
Alpha (8–12 Hz)	lvPPA versus nfvPPA	0.16 (0.69)	13.46 (0.001)	6.83 (0.01)
	svPPA versus lvPPA	1.28 (0.26)	237.84 (<0.0001)	4.19 (0.04)
	svPPA versus nfvPPA	0.30 (0.59)	92.51 (<0.0001)	4.53 (0.04)
Beta (12–30 Hz)	lvPPA versus nfvPPA	6.29 (0.02)	68.64 (<0.0001)	17.68 (0.0001)
	svPPA versus lvPPA	4.70 (0.03)	199.92 (<0.0001)	7.97 (0.01)
	svPPA versus nfvPPA	0.00 (0.99)	80.82 (<0.0001)	22.63 (<0.0001)
Delta-theta (2–8 Hz)	lvPPA versus nfvPPA	5.46 (0.02)	2.23 (0.14)	0.18 (0.68)
	svPPA versus lvPPA	16.10 (0.0002)	29.75 (<0.0001)	1.65 (0.21)
	svPPA versus nfvPPA	0.83 (0.37)	14.43 (0.0004)	0.02 (0.88)

Table shows the F- and *P*-values for two-way ANOVA analyses examining whether the distinct patterns of functional connectivity observed in each PPA variant against age-matched controls are different between the PPA variants themselves. Each pairwise comparison at each frequency was included in a general linear model. The two factors in the ANOVA model included the region-of-interest identity (variant-specific region of interest identity) and the PPA variant identity.

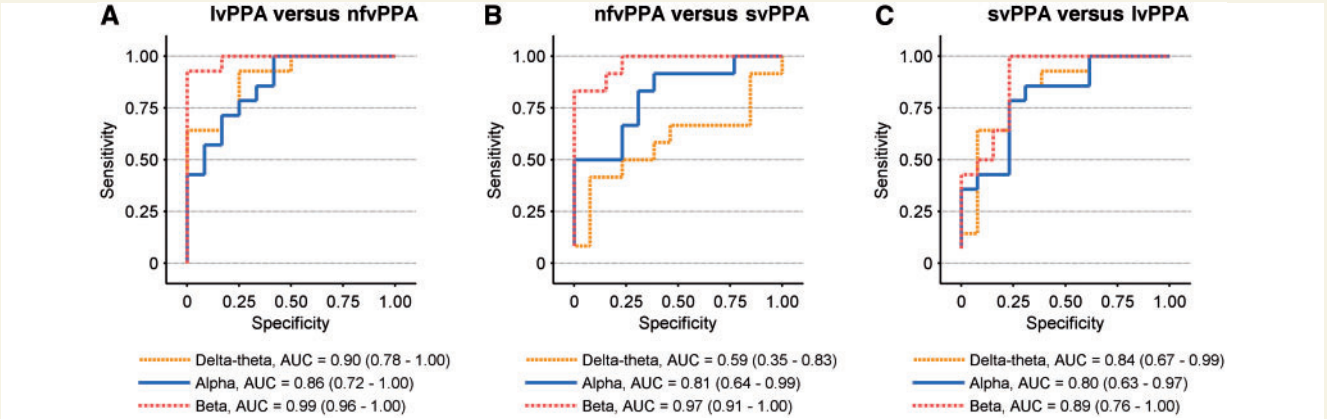

Figure 3 Receiver operating characteristic (ROC) curves based on functional connectivity patterns. The subplots display the ROC curves derived from logistic regression analysis depicting the discriminability between pairs of PPA variants: (**A**) lvPPA versus nfvPPA; (**B**) nfvPPA versus svPPA (**C**) svPPA versus lvPPA. Each subplot displays three ROC curves representing: delta-theta (2–8 Hz; yellow line); alpha (2–8 Hz; blue line); beta (12–30 Hz; red line). In each logistic regression analysis, the imaginary coherence of the two PPA variants compared against each other consisted the predictor variables of the model. The imaginary coherence values at each frequency for each group represented the average across the voxel clusters of the respective anatomic regions as depicted in Fig. 1. The legends for each subplot show the area under the curve (AUC) and the confidence intervals within parentheses, for the ROC curves.

(Fig. 4C and Supplementary Table 3). The beta power was also reduced in svPPA patients and was limited to the left anterior temporal lobe (Fig. 4C and Supplementary Table 3). In contrast to functional connectivity deficits of alpha and beta bands, which were consistently independent of cortical atrophy, the spectral power differences showed partial dependencies on cortical volumes. For example, lvPPA was the only group that showed atrophy-independent spectral power changes in both alpha and beta bands (Fig. 5A). Except for the alpha power in nfvPPA, other spectral power differences in nfvPPA and svPPA were no longer significant when corrected for cortical grey matter volume loss (Fig. 5B and C).

Increased delta-theta spectral power in logopenic variant PPA

Within delta-theta frequency lvPPA patients showed increased spectral power specifically involving the frontal lobes, bilaterally (Fig. 4A and Supplementary Table 3). Patients with nfvPPA showed a cluster of voxels with increased power over the left temporal pole and reduced power in right posterior-inferior frontal gyrus and adjacent regions, while svPPA patients showed reduced delta-theta power in bilateral temporal lobes (Fig. 4B and C and Supplementary Table 3). However, the power changes in both nfvPPA and svPPA were no longer significant when corrected for cortical grey

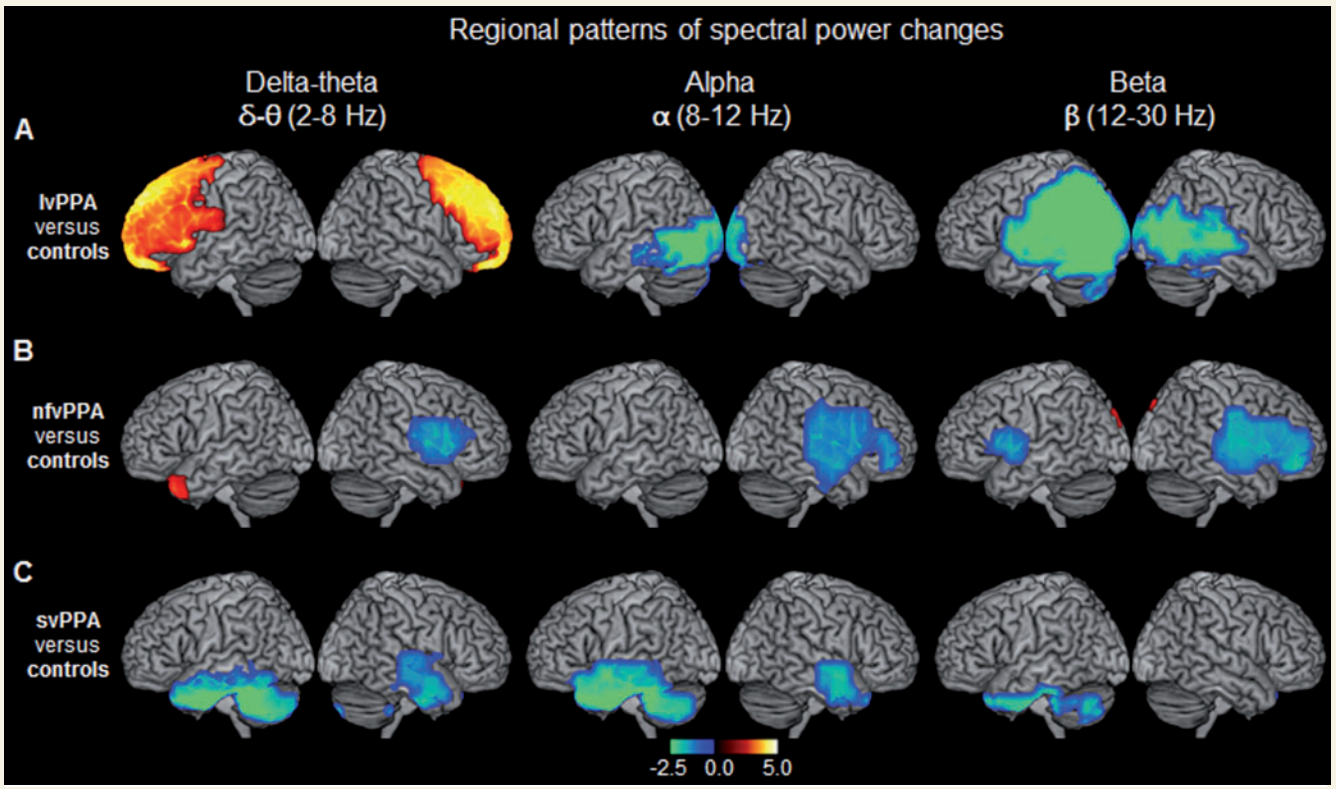

Figure 4 Spatiotemporal patterns of spectral power distribution in each PPA variant compared to age-matched controls. The rendering brain images depict the distinct patterns of spectral power density for each frequency, in the three PPA variants when compared to age-matched controls. (**A**) lvPPA versus controls; (**B**) nfvPPA versus controls; (**C**) svPPA versus controls. Colours indicate the *t*-values depicting statistically significant patterns of increased (hot colours) and decreased (cold colours) spectral power within each frequency. From left to right columns represent the frequency bands: delta-theta (2–8 HZ); alpha (8–12 Hz); beta (12–30 Hz), respectively. Images are statistically thresholded using cluster correction (20 voxels cut-off) and $P < 0.001$ for lvPPA, $P < 0.01$ for svPPA and $P < 0.05$ for nfvPPA ($n = 14$ lvPPA; $n = 13$ svPPA; $n = 12$ nfvPPA; $n = 20$ controls).

matter volume (Fig. 5B and C), indicating that these effects cannot be ruled as independent of the distinctions created by distinct atrophy patterns. In contrast, the increased delta-theta spectral power of lvPPA remained significant even after correcting for grey matter volume (Fig. 5A). Taken together with increased imaginary coherence patterns shown earlier, lvPPA is distinctly characterized by congruent delta-theta hypersynchrony and hyperactivity.

Discussion

This study is the first to examine direct spontaneous neural activity patterns as captured by MEGI across the three main variants of PPA: lvPPA, svPPA, and nfvPPA. We leveraged the high temporal resolution of MEGI and used novel, unbiased, whole-brain methodology to compute functional connectivity of neuronal oscillations at rest. We demonstrated: (i) distinct spatiotemporal patterns with network-specific hyposynchrony of alpha and beta bands in each PPA variant and (ii) congruent hypersynchrony and hyperactivity of delta-theta oscillations specific to lvPPA patients. Our findings suggest that altered patterns of neuronal synchrony may relate to distinct pathophysiological processes in each PPA variant, and is consistent with theoretical and empirical models of network degeneration that propose phenotypic variations are modulated by specific proteinopathies (Drzezga *et al.*, 2011; Sepulcre *et al.*, 2013; Warren *et al.*, 2013).

Synchronous oscillations entail the functional constructs interfacing cellular processes and system-level activity (Buzsaki, 2011; Buzsaki *et al.*, 2012). Different oscillatory frequencies are generated by specific intrinsic properties of neuronal circuits including local and long-range, as well as excitatory and inhibitory connections (Sohal *et al.*, 2009; Wang, 2010). While pathological mechanisms leading to network dysfunction in neurodegeneration are currently not yet fully understood, recent experimental and theoretical works have generated important mechanistic insights. Below we discuss results of the current MEGI study in PPA in the context of recent developments in pathophysiology of network dysfunction in focal neurodegenerative diseases.

Distinct spatiotemporal patterns of connectivity deficits in PPA

Our results demonstrate distinctive spatial patterns of hyper- and hypo-synchrony in each PPA variant. Specifically, the current study identifies alpha and beta

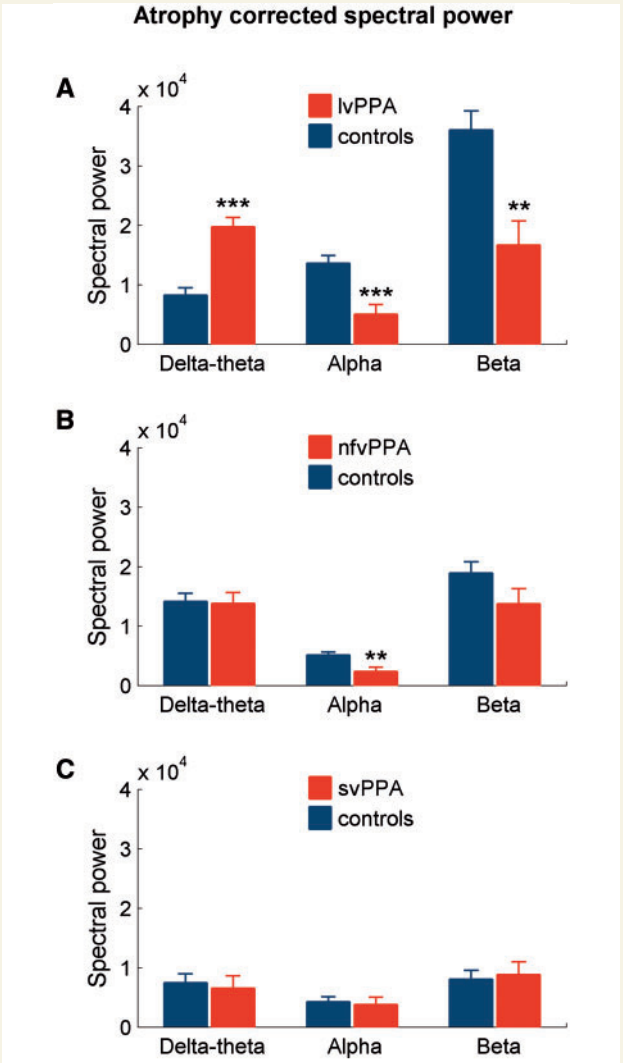

Figure 5 Patterns of spectral power differences after correcting for cortical atrophy. The bar plots depict the results from general linear model analysis of spectral power values including the cortical grey matter volumes as a covariate, comparing each PPA variant and controls, for each frequency. The stars indicate statistically significant differences between patients and controls at each frequency. (**A**) lvPPA versus controls; (**B**) nfvPPA versus controls; (**C**) svPPA versus controls. $^{**}P < 0.01$; $^{***}P < 0.001$.

neural synchronizations (8–12 Hz and 12–30 Hz) as the most dysfunctional pattern across all three PPA variants, thus providing a common functional substrate underlying language disability, albeit within different brain areas recruited for language function. Previous MEGI studies on healthy populations have demonstrated 8–30 Hz oscillation to show the most salient synchronized patterns within, as well as between, resting state functional networks (de Pasquale *et al.*, 2010, 2012). In this context, our results demonstrate that regional specificity of neurodegenerative diseases is integrally related to intrinsic network architecture of the resting brain. MEGI-derived alpha and beta hyposynchrony in PPA variants remained robust even after correcting for grey matter volumes. This result is consistent with the idea that functional disruptions of neural networks is separated in space and time from structural disruptions (Jagust, 2013*b*). A wealth of evidence also supports the hypothesis that functional circuits become disorganized early in the disease process and may precede structural changes by several years (Jagust, 2013*a*). Identification of syndrome-specific functional connectivity deficits thus may indicate the earliest manifestations of network dysfunctions.

Studies of functional connectivity have transformed our approach to neurodegenerative diseases. The classic view that the structural damage underlies cognitive impairment via reduced cortical activity is challenged by recent neuroimaging studies demonstrating functional modulations of spatially distributed neural networks. The framework of selective network vulnerability (Seeley *et al.*, 2009; Pievani *et al.*, 2011; Mattsson *et al.*, 2016), suggests that pathophysiological consequences of neurodegenerative diseases reflect the interplay of network-specific factors that determine targeted circuits and disease-specific factors that determine molecular pathology. It is known that each variant of PPA is associated with higher probability of a specific molecular change at the cellular level, with Alzheimer's disease being the most common in lvPPA, frontotemporal lobar degeneration (FTLD)-tau in nfvPPA and FTLD-TDP in svPPA (Mesulam *et al.*, 2014). In our cohort, Alzheimer's disease biomarkers were tested in 12 of 14 lvPPA and in all nfvPPA patients. All lvPPA patients tested for Alzheimer's disease biomarkers showed positive results (i.e. positive amyloid imaging in positron emission tomography or reduced amyloid-β42/Tau index in CSF), while all nfvPPA patients were negative. In the following discussion, we therefore relate our findings to known Alzheimer's disease biology in lvPPA and speculate that the unique patterns of functional connectivity deficits in nfvPPA and svPPA may relate to the most common FTLD proteinopathies associated with each PPA syndrome (Spinelli *et al.*, 2017).

Network hypersynchrony and hyperactivity in logopenic variant PPA

MEGI revealed that lvPPA variant was the only group associated with both hypersynchrony and hyperactivity of delta-theta. The most common reported underlying pathology in lvPPA is Alzheimer's disease (Mesulam *et al.*, 2008; Rabinovici *et al.*, 2008; Teichmann *et al.*, 2013; Spinelli *et al.*, 2017). Animal models of Alzheimer's disease as well as human functional neuroimaging have provided compelling evidence that network hyperactivity plays a key role in the pathogenesis of Alzheimer's disease-related cognitive dysfunction (Huijbers *et al.*, 2015; Palop and Mucke, 2016). Spontaneous epileptiform activity has been documented in Alzheimer's disease patients at early stages (Vossel *et al.*, 2013, 2016), and also in different animal

models of familial Alzheimer's disease (Palop *et al.*, 2007; Harris *et al.*, 2010; Um *et al.*, 2012). In transgenic mice, the network hyperexcitability and related cognitive behavioural deficits have been attributed to toxic molecular effects of soluble amyloid-β. The hyperactive and hypersynchronous delta-theta that we detected in lvPPA patients provide an *in vivo* biomarker of analogous Alzheimer's disease-related pathophysiology in human disease. Network hypersynchrony has also been observed on resting state functional MRI in cognitively normal individuals with PET evidence for amyloid-β deposition (Schultz *et al.*, 2017), suggesting this could be an early phenomenon in Alzheimer's disease. Since specific frequency oscillations explicitly recruit highly specialized inhibitory interneurons (Wang, 2010), selective disruption of oscillatory patterns may relate to dysfunction of specific neuronal subtypes. The low frequency delta-theta oscillations of hippocampus, in fact, have shown to be predominantly modulated by cholecystokinin-expressing perisomatic inhibitory interneurons and by dendrite-targeting GABAergic cells (Klausberger and Somogyi, 2008). Future experiments in animal models of Alzheimer's disease exploring these specific cellular abnormalities will provide critical information to bridge the gap between molecular and network anomalies in Alzheimer's disease.

Distinct patterns of frontal hyposynchrony in non-fluent/agrammatic variant PPA

Previous studies have demonstrated compelling evidence that motor speech and grammatical deficits in nfvPPA are associated with deficits in the left fronto-insular-striatal structures involved in speech production (Mandelli *et al.*, 2014). Consistent with this observation, our current results demonstrated a similar anatomic distribution of alpha and beta hyposynchrony (8–30 Hz) in nfvPPA. Given that post-mortem pathological changes underlying nfvPPA are most often FTLD-tau (Mesulam *et al.*, 2008; Grossman, 2010; Spinelli *et al.*, 2017) one could speculate that the downstream effects of tau changes in nfvPPA selectively manifests in circuit properties responsible of producing 8–30 Hz oscillations. Pathological tau could mediate synaptic dysfunction in the local neuronal populations that participate in these oscillations prior to overt loss of synapses (Hoover *et al.*, 2010). Previous MEG studies on frontotemporal dementia patients, a disease that often involves FTLD-tau, has also shown reduced beta frequency connectivity within left frontotemporal interactions (Hughes and Rowe, 2013).

NfvPPA and lvPPA showed strikingly different patterns of MEGI-derived functional connectivity and spectral activity. Although the diagnostic classification of PPA published in 2011 clearly distinguish the clinical and neuroanatomical features of these two PPA presentations, their early differential diagnosis in clinical practice remains challenging (Gorno-Tempini *et al.*, 2011; Sajjadi *et al.*, 2012). Indeed, both syndromes present with errors in speech production and initial subtle anatomical changes. Explicit differences detected by MEGI between these two variants therefore are of particular clinical significance. The most salient distinction was the congruent hypersynchrony and hyperactivity in lvPPA patients within the low frequency delta-theta, which was absent in nfvPPA. MEGI-derived low frequency oscillatory patterns hence may provide a useful tool for differential diagnosis between lvPPA and nfvPPA, likely in relation to the above mentioned Alzheimer's disease pathology in lvPPA.

Distributed functional connectivity deficits in semantic variant PPA

Semantic variant PPA is characterized by word and object knowledge impairment, and spared phonology and grammar in association with temporal polar atrophy (Gorno-Tempini *et al.*, 2004, 2011; Mesulam *et al.*, 2009). Consistent with the severe anatomical damage of anterior temporal lobe, spectral power analysis in svPPA showed decreased activity in all frequency bands that was related to volume loss. Instead, synchrony analyses showed specific severe changes in the alpha and beta connectivity in the posterior language network, which is not usually structurally damaged in svPPA. The combination of these structural and functional changes provides useful insights into the organization of the language system and the pathophysiology of svPPA.

The relative role of the left anterior temporal lobe in semantic and language networks has been a matter of active debate in cognitive neuroscience and behavioural neurology. In classic aphasiology, consistent with the distribution of lesions in stroke aphasia, the language network comprises left perisylvian regions (Hillis, 2007; Price, 2012). In such context, lesions of the posterior temporal and inferior parietal regions were associated with word comprehension and retrieval deficits. The description of the severe word and object knowledge deficits in svPPA have challenged this view and supported a cognitive-anatomical model in which the anterior temporal lobe is a fundamental region within the language network, functioning as a semantic hub that links linguistic and perceptual features into a coherent mental representation (Patterson *et al.*, 2007). However, the effect of anterior temporal lobe atrophy on the rest of the language network is still a matter of debate. Recent functional MRI studies provide evidence for altered connectivity related to modality-specific associations between anterior temporal lobe and the rest of the temporal cortex in svPPA, suggesting that anterior temporal lobe atrophy may cause widespread alteration in a distributed semantic network (Goll *et al.*, 2012; Hurley *et al.*, 2015). The current study expands these findings and identifies the left posterior superior temporal and adjacent inferior parietal cortex to be the region with most severely disrupted alpha-beta synchrony in svPPA, likely in relation to its

connectivity to the damaged left anterior temporal lobe. Collectively these results indicate that the structural loss of neurons and synapses in the left anterior temporal lobe is strongly associated with the functional disruption of left posteriori perisylvian language cortices. The current results therefore provide a unitary framework between classic neurological models of aphasia and modern cognitive neuroscience approaches by showing that svPPA is characterized by anterior temporal lobe structural damage and left perisylvian functional damage.

In the past decade, svPPA has been reliably associated with FTLD-TDP-43 (TAR DNA-binding protein 43) deposition in post-mortem assessments. The strong impact of atrophy on spectral power in svPPA suggests that local reductions in alpha and beta activity relate to structural changes in TDP-43 disorders, possibly more so than in other proteinopathies. The potential influence of TDP-43, which is normally a nuclear protein, on neuronal activity or on synaptic function is less understood than that of amyloid-β and tau. Studying svPPA patients in early stage of the disease hence would be useful to understand the specific network alterations that precede neuronal loss. As further evidence emergences regarding the biological mechanisms of TDP-related neurodegeneration, we will be able to relate MEG findings to possible neurophysiological mechanisms.

Limitations and future studies

The current analyses were limited to identify distinct patterns of neural oscillatory changes in each PPA variant compared to an age-matched control group. Although our region of interest-based direct comparisons between PPA variants indicated reliable differences, given the scope of this paper, we did not extend our analyses into direct, whole-brain comparisons between PPA variants. The region of interest-based logistic regression analysis we present in this paper quantifies the differences within specific anatomic regions identified from the comparisons against controls, and does not provide a diagnostic metric for differential diagnoses between PPA variants. Future studies designed to compare the spatiotemporal characteristics directly between the PPA variants themselves will greatly improve our understanding of relative strengths and weaknesses of regional networks in each syndrome. Another important challenge for future studies is to clearly identify the cellular and molecular mechanisms mediating altered patterns of neuronal synchronizations in focal neurodegenerative diseases. Furthermore, although previous experiments have shown that the methods used in our analyses—adaptive spatial filtering and imaginary coherence—yield consistent results with high reliability, future studies based on other source localization methods and functional connectivity metrics (Colclough *et al.*, 2016) will extend our knowledge about electrophysiological signatures of disrupted functional networks.

Conclusion

MEGI provides a valuable tool to characterize the resting state electrophysiological signatures in each PPA syndrome. Network dysfunction in neurodegenerative diseases provides a framework for further studies examining cognitive correlates of electrophysiological changes and prediction of longitudinal course as well as pathophysiological mechanisms of brain proteinopathies.

Acknowledgements

We would like to thank all of the study participants and their families for their generous support to our research. We would like to thank Dr Iryna Lobach for her expert guidance on statistical analyses.

Funding

This study was supported by the National Institutes of Health grants: R01NS050915 (M.L.G.T.), K24DC015544 (M.L.G.T.), U01AG052943 (M.L.G.T.), F32AG050434-01A1 (K.G.R.), K23 AG038357 (K.A.V.), P50 AG023501 (B.L.M.), P01 AG19724 (B.L.M.), R21 NS76171 (S.S.N.), R01 DC010145 (J.F.H.), DC013979 (S.S.N.), R01 NS066654 (S.S.N.), R01 NS64060 (S.S.N.), R01 NS100440 (S.S.N.), 2R01AG038791-06A1 (A.L.B.), U54NS092089 (A.L.B.), National Science Foundation Grant BCS-1262297 (S.S.N.); a grant from John Douglas French Alzheimer's Foundation (K.A.V.); a grant from Larry L. Hillblom Foundation, 2015-A-034-FEL (K.G.R.); University of California San Francisco Alzheimer's Disease Research Center pilot project grant (K.A.V.); grants from the Alzheimer's Association and made possible by Part the CloudTM,: (PCTRB-13-288476) (K.A.V.), ETAC-09-133596 (J.F.H.); and a gift from the S. D. Bechtel Jr. Foundation (.K.A.V), and a gift from Ricoh Inc. (S.S.N.). K.G.R., L.B.H., A.J.B., S.H., D.M., G.C., A.L., A.E.W., I.H., Z.A.M., M.L.M., M.L.G.T., A.L.B., K.A.V., S.S.N. and J.F.H. declare no competing financial interests relevant for this work. B.L.M. has the following disclosures: serves as Medical Director for the John Douglas French Foundation; Scientific Director for the Tau Consortium; Director/Medical Advisory Board of the Larry L. Hillblom Foundation; and Scientific Advisory Board Member for the National Institute for Health Research Cambridge Biomedical Research Centre and its subunit, the Biomedical Research Unit in Dementia, UK.

Supplementary material

Supplementary material is available at *Brain* online.

References

Barnes GR, Hillebrand A, Fawcett IP, Singh KD. Realistic spatial sampling for MEG beamformer images. Hum Brain Mapp 2004; 23: 120–7.

Bullmore E, Sporns O. Complex brain networks: graph theoretical analysis of structural and functional systems. Nat Rev Neurosci 2009; 10: 186–98.

Buzsaki G. Rhythms of the brain. New York, NY: Oxford University Press; 2011.

Buzsaki G, Anastassiou CA, Koch C. The origin of extracellular fields and currents–EEG, ECoG, LFP and spikes. Nat Rev Neurosci 2012; 13: 407–20.

Colclough GL, Woolrich MW, Tewarie PK, Brookes MJ, Quinn AJ, Smith SM. How reliable are MEG resting-state connectivity metrics? Neuroimage 2016; 138: 284–93.

Dalal SS, Guggisberg AG, Edwards E, Sekihara K, Findlay AM, Canolty RT, et al. Five-dimensional neuroimaging: localization of the time-frequency dynamics of cortical activity. Neuroimage 2008; 40: 1686–700.

Dalal SS, Zumer JM, Guggisberg AG, Trumpis M, Wong DD, Sekihara K, et al. MEG/EEG source reconstruction, statistical evaluation, and visualization with NUTMEG. Comput Intell Neurosci 2011; 2011: 758973.

de Pasquale F, Della Penna S, Snyder AZ, Lewis C, Mantini D, Marzetti L, et al. Temporal dynamics of spontaneous MEG activity in brain networks. Proc Natl Acad Sci USA 2010; 107: 6040–5.

de Pasquale F, Della Penna S, Snyder AZ, Marzetti L, Pizzella V, Romani GL, et al. A cortical core for dynamic integration of functional networks in the resting human brain. Neuron 2012; 74: 753–64.

Drzezga A, Becker JA, Van Dijk KR, Sreenivasan A, Talukdar T, Sullivan C, et al. Neuronal dysfunction and disconnection of cortical hubs in non-demented subjects with elevated amyloid burden. Brain 2011; 134(Pt 6): 1635–46.

Engel AK, Gerloff C, Hilgetag CC, Nolte G. Intrinsic coupling modes: multiscale interactions in ongoing brain activity. Neuron 2013; 80: 867–86.

Galantucci S, Tartaglia MC, Wilson SM, Henry ML, Filippi M, Agosta F, et al. White matter damage in primary progressive aphasias: a diffusion tensor tractography study. Brain 2011; 134(Pt 10): 3011–29.

Goll JC, Ridgway GR, Crutch SJ, Theunissen FE, Warren JD. Nonverbal sound processing in semantic dementia: a functional MRI study. Neuroimage 2012; 61: 170–80.

Gorno-Tempini ML, Brambati SM, Ginex V, Ogar J, Dronkers NF, Marcone A, et al. The logopenic/phonological variant of primary progressive aphasia. Neurology 2008; 71: 1227–34.

Gorno-Tempini ML, Dronkers NF, Rankin KP, Ogar JM, Phengrasamy L, Rosen HJ, et al. Cognition and anatomy in three variants of primary progressive aphasia. Ann Neurol 2004; 55: 335–46.

Gorno-Tempini ML, Hillis AE, Weintraub S, Kertesz A, Mendez M, Cappa SF, et al. Classification of primary progressive aphasia and its variants. Neurology 2011; 76: 1006–14.

Grossman M. Primary progressive aphasia: clinicopathological correlations. Nat Rev Neurol 2010; 6: 88–97.

Grossman M. The non-fluent/agrammatic variant of primary progressive aphasia. Lancet Neurol 2012; 11: 545–55.

Guggisberg AG, Honma SM, Findlay AM, Dalal SS, Kirsch HE, Berger MS, et al. Mapping functional connectivity in patients with brain lesions. Ann Neurol 2008; 63: 193–203.

Guo CC, Gorno-Tempini ML, Gesierich B, Henry M, Trujillo A, Shany-Ur T, et al. Anterior temporal lobe degeneration produces widespread network-driven dysfunction. Brain 2013; 136(Pt 10): 2979–91.

Harris AZ, Gordon JA. Long-range neural synchrony in behavior. Annu Rev Neurosci 2015; 38: 171–94.

Harris JA, Devidze N, Verret L, Ho K, Halabisky B, Thwin MT, et al. Transsynaptic progression of amyloid-beta-induced neuronal dysfunction within the entorhinal-hippocampal network. Neuron 2010; 68: 428–41.

Hillis AE. Aphasia: progress in the last quarter of a century. Neurology 2007; 69: 200–13.

Hinkley LB, Marco EJ, Findlay AM, Honma S, Jeremy RJ, Strominger Z, et al. The role of corpus callosum development in functional connectivity and cognitive processing. PLoS One 2012; 7: e39804.

Hinkley LB, Owen JP, Fisher M, Findlay AM, Vinogradov S, Nagarajan SS. Cognitive impairments in schizophrenia as assessed through activation and connectivity measures of magnetoencephalography (MEG) data. Front Hum Neurosci 2010; 3: 73.

Hoover BR, Reed MN, Su J, Penrod RD, Kotilinek LA, Grant MK, et al. Tau mislocalization to dendritic spines mediates synaptic dysfunction independently of neurodegeneration. Neuron 2010; 68: 1067–81.

Hughes LE, Rowe JB. The impact of neurodegeneration on network connectivity: a study of change detection in frontotemporal dementia. J Cogn Neurosci 2013; 25: 802–13.

Huijbers W, Mormino EC, Schultz AP, Wigman S, Ward AM, Larvie M, et al. Amyloid-beta deposition in mild cognitive impairment is associated with increased hippocampal activity, atrophy and clinical progression. Brain 2015; 138(Pt 4): 1023–35.

Hurley RS, Bonakdarpour B, Wang X, Mesulam MM. Asymmetric connectivity between the anterior temporal lobe and the language network. J Cogn Neurosci 2015; 27: 464–73.

Jagust W. Biomarkers and brain connectivity. JAMA Neurol 2013a; 70: 1233–4.

Jagust W. Vulnerable neural systems and the borderland of brain aging and neurodegeneration. Neuron 2013b; 77: 219–34.

Khan S, Gramfort A, Shetty NR, Kitzbichler MG, Ganesan S, Moran JM, et al. Local and long-range functional connectivity is reduced in concert in autism spectrum disorders. Proc Natl Acad Sci USA 2013; 110: 3107–12.

Klausberger T, Somogyi P. Neuronal diversity and temporal dynamics: the unity of hippocampal circuit operations. Science 2008; 321: 53–7.

Kort NS, Cuesta P, Houde JF, Nagarajan SS. Bihemispheric network dynamics coordinating vocal feedback control. Hum Brain Mapp 2016; 37: 1474–85.

Kramer JH, Jurik J, Sha SJ, Rankin KP, Rosen HJ, Johnson JK, et al. Distinctive neuropsychological patterns in frontotemporal dementia, semantic dementia, and Alzheimer disease. Cogn Behav Neurol 2003; 16: 211–8.

Lehmann M, Ghosh PM, Madison C, Laforce R, Jr., Corbetta-Rastelli C, Weiner MW, et al. Diverging patterns of amyloid deposition and hypometabolism in clinical variants of probable Alzheimer's disease. Brain 2013; 136(Pt 3): 844–58.

Leyton CE, Britton AK, Hodges JR, Halliday GM, Kril JJ. Distinctive pathological mechanisms involved in primary progressive aphasias. Neurobiol Aging 2016; 38: 82–92.

Mandelli ML, Caverzasi E, Binney RJ, Henry ML, Lobach I, Block N, et al. Frontal white matter tracts sustaining speech production in primary progressive aphasia. J Neurosci 2014; 34: 9754–67.

Martino J, Honma SM, Findlay AM, Guggisberg AG, Owen JP, Kirsch HE, et al. Resting functional connectivity in patients with brain tumors in eloquent areas. Ann Neurol 2011; 69: 521–32.

Mattsson N, Schott JM, Hardy J, Turner MR, Zetterberg H. Selective vulnerability in neurodegeneration: insights from clinical variants of Alzheimer's disease. J Neurol Neurosurg Psychiatry 2016; 87: 1000–4.

Mesulam M, Rogalski E, Wieneke C, Cobia D, Rademaker A, Thompson C, et al. Neurology of anomia in the semantic variant of primary progressive aphasia. Brain 2009; 132(Pt 9): 2553–65.

Mesulam M, Wicklund A, Johnson N, Rogalski E, Leger GC, Rademaker A, et al. Alzheimer and frontotemporal pathology in

subsets of primary progressive aphasia. Ann Neurol 2008; 63: 709–19.
Mesulam MM. Primary progressive aphasia. Ann Neurol 2001; 49: 425–32.
Mesulam MM. Primary progressive aphasia—a language-based dementia. N Engl J Med 2003; 349: 1535–42.
Mesulam MM, Rogalski EJ, Wieneke C, Hurley RS, Geula C, Bigio EH, et al. Primary progressive aphasia and the evolving neurology of the language network. Nat Rev Neurol 2014; 10: 554–69.
Nolte G, Bai O, Wheaton L, Mari Z, Vorbach S, Hallett M. Identifying true brain interaction from EEG data using the imaginary part of coherency. Clin Neurophysiol 2004; 115: 2292–307.
Ossenkoppele R, Schonhaut DR, Scholl M, Lockhart SN, Ayakta N, Baker SL, et al. Tau PET patterns mirror clinical and neuroanatomical variability in Alzheimer's disease. Brain 2016; 139(Pt 5): 1551–67.
Palop JJ, Chin J, Roberson ED, Wang J, Thwin MT, Bien-Ly N, et al. Aberrant excitatory neuronal activity and compensatory remodeling of inhibitory hippocampal circuits in mouse models of Alzheimer's disease. Neuron 2007; 55: 697–711.
Palop JJ, Mucke L. Network abnormalities and interneuron dysfunction in Alzheimer disease. Nat Rev Neurosci 2016; 17: 777–92.
Patterson K, Nestor PJ, Rogers TT. Where do you know what you know? The representation of semantic knowledge in the human brain. Nat Rev Neurosci 2007; 8: 976–87.
Pievani M, de Haan W, Wu T, Seeley WW, Frisoni GB. Functional network disruption in the degenerative dementias. Lancet Neurol 2011; 10: 829–43.
Price CJ. A review and synthesis of the first 20 years of PET and fMRI studies of heard speech, spoken language and reading. Neuroimage 2012; 62: 816–47.
Rabinovici GD, Jagust WJ, Furst AJ, Ogar JM, Racine CA, Mormino EC, et al. Abeta amyloid and glucose metabolism in three variants of primary progressive aphasia. Ann Neurol 2008; 64: 388–401.
Ranasinghe KG, Hinkley LB, Beagle AJ, Mizuiri D, Dowling AF, Honma SM, et al. Regional functional connectivity predicts distinct cognitive impairments in Alzheimer's disease spectrum. Neuroimage Clin 2014; 5: 385–95.
Ranasinghe KG, Rankin KP, Lobach IV, Kramer JH, Sturm VE, Bettcher BM, et al. Cognition and neuropsychiatry in behavioral variant frontotemporal dementia by disease stage. Neurology 2016; 86: 600–10.
Sajjadi SA, Patterson K, Arnold RJ, Watson PC, Nestor PJ. Primary progressive aphasia: a tale of two syndromes and the rest. Neurology 2012; 78: 1670–7.
Schultz AP, Chhatwal JP, Hedden T, Mormino EC, Hanseeuw BJ, Sepulcre J, et al. Phases of hyperconnectivity and hypoconnectivity in the default mode and salience networks track with amyloid and tau in clinically normal individuals. J Neurosci 2017; 37: 4323–31.
Seeley WW, Crawford RK, Zhou J, Miller BL, Greicius MD. Neurodegenerative diseases target large-scale human brain networks. Neuron 2009; 62: 42–52.
Sepulcre J, Sabuncu MR, Becker A, Sperling R, Johnson KA. *In vivo* characterization of the early states of the amyloid-beta network. Brain 2013; 136(Pt 7): 2239–52.
Sohal VS, Zhang F, Yizhar O, Deisseroth K. Parvalbumin neurons and gamma rhythms enhance cortical circuit performance. Nature 2009; 459: 698–702.
Sonty SP, Mesulam MM, Weintraub S, Johnson NA, Parrish TB, Gitelman DR. Altered effective connectivity within the language network in primary progressive aphasia. J Neurosci 2007; 27: 1334–45.
Spinelli EG, Mandelli ML, Miller ZA, Santos-Santos MA, Wilson SM, Agosta F, et al. Typical and atypical pathology in primary progressive aphasia variants. Ann Neurol 2017; 81: 430–43.
Teichmann M, Kas A, Boutet C, Ferrieux S, Nogues M, Samri D, et al. Deciphering logopenic primary progressive aphasia: a clinical, imaging and biomarker investigation. Brain 2013; 136(Pt 11): 3474–88.
Um JW, Nygaard HB, Heiss JK, Kostylev MA, Stagi M, Vortmeyer A, et al. Alzheimer amyloid-beta oligomer bound to postsynaptic prion protein activates Fyn to impair neurons. Nat Neurosci 2012; 15: 1227–35.
Vossel KA, Beagle AJ, Rabinovici GD, Shu H, Lee SE, Naasan G, et al. Seizures and epileptiform activity in the early stages of Alzheimer disease. JAMA Neurol 2013; 70: 1158–66.
Vossel KA, Ranasinghe KG, Beagle AJ, Mizuiri D, Honma SM, Dowling AF, et al. Incidence and impact of subclinical epileptiform activity in Alzheimer's disease. Ann Neurol 2016; 80: 858–70.
Wang XJ. Neurophysiological and computational principles of cortical rhythms in cognition. Physiol Rev 2010; 90: 1195–268.
Warren JD, Rohrer JD, Schott JM, Fox NC, Hardy J, Rossor MN. Molecular nexopathies: a new paradigm of neurodegenerative disease. Trends Neurosci 2013; 36: 561–9.
Wilson SM, Dronkers NF, Ogar JM, Jang J, Growdon ME, Agosta F, et al. Neural correlates of syntactic processing in the nonfluent variant of primary progressive aphasia. J Neurosci 2010; 30: 16845–54.